REPORT DOCUMENTATION PAGE

AFRL-SR-AR-TR-04-
0264

1. AGENCY USE ONLY *(Leave blank)*	2. REPORT DATE	3. REPORT
	April 2004	Final Technical Report (01 Mar 03 - 31 Dec 03)

4. TITLE AND SUBTITLE
Correlation of Flow Structures and Radiated Noise in High Speed Jets

5. FUNDING NUMBERS
F49620-03-1-0154
2307/AX
61102F

6. AUTHOR(S)
M. Samimy, J. Hileman, E. Caraballo, and B. Thurow

7. PERFORMING ORGANIZATION NAME(S) AND ADDRESS(ES)
The Ohio State University
Gas Dynamics and Turbulence Laboratory
Dept of Mechanical Engineering
Columbus, OH 43210

8. PERFORMING ORGANIZATION REPORT NUMBER

9. SPONSORING/MONITORING AGENCY NAME(S) AND ADDRESS(ES)
AFOSR/NA
4015 Wilson Blvd., Room 713
Arlington, VA 22230-1954
Program Manager: Dr. John Schmisseur

10. SPONSORING/MONITORING AGENCY REPORT NUMBER

11. SUPPLEMENTARY NOTES

12a. DISTRIBUTION AVAILABILITY STATEMENT
APPROVED FOR PULBIC RELEASE, DISTRIBUTION IS UNLIMITED

12b. DISTRIBUTION CODE

13. ABSTRACT *(Maximum 200 words)*

The dynamics of large-scale turbulence structures within a high Reynolds number, ideally expanded Mach 1.3 jet were investigated during both the periods of production of strong acoustic radiation and extended periods of relative quiet that lacked such acoustic radiation. These results were acquired through a unique experiment where the sources of large amplitude sound waves were estimated with a three-dimensional microphone array and the flow field was simultaneously visualized on two orthogonal planes. The images from one of the planes were taken at a 167 kHz rate. Proper Orthogonal Decomposition (POD) was employed to create a basis of the size and distribution of large-scale structures within the two planes. These POD modes were then used to objectively determine the differences in the jet structure during noise generation and periods lacking significant noise generation. The results show that the flow during the periods of relative quiet cases is dominated by the lower order POD modes that consist of relatively large turbulence structures while it is dominated by higher order POD modes that capture the dynamic interplay of the large-scale structures during noise generation periods. For approximately one convective time scale prior to the moment of noise emission, a series of large-scale structures forms and disintegrates within the mixing layer and in the process a large amount of ambient fluid is entrained into the core of the jet. For the first time, these results show how the dynamic interplay of large-scale turbulence structures generates acoustic radiation within a high Reynolds number jet.

14. SUBJECT TERMS			15. NUMBER OF PAGES 28
			16. PRICE CODE
17. SECURITY CLASSIFICATION OF REPORT	18. SECURITY CLASSIFICATION OF THIS PAGE	19. SECURITY CLASSIFICATION OF ABSTRACT	20. LIMITATION OF ABSTRACT
U	U	U	

Correlation of Flow Structures and Radiated Noise in High Speed Jets

M. Samimy, J. Hileman, E. Caraballo, and B. Thurow
Gas Dynamics and Turbulence Laboratory
Department of Mechanical Engineering
The Ohio State University
Columbus, Ohio 43210

Final Technical Report
(GDTL 1-2004)

For

AFOSR Grant F49620-03-1-0154

For the Period of

March 1, 2003 – December 31, 2003

April 2004

Correlation of Flow Structures and Radiated Noise in High Speed Jets

M. Samimy[1], J. Hileman[2], E. Caraballo[2], and B. Thurow[2]
Gas Dynamics and Turbulence Laboratory
Department of Mechanical Engineering
The Ohio State University
Columbus, Ohio 43210

Final Technical Report
(GDTL 1-2004)

For

AFOSR Grant F49620-03-1-0154

For the Period of

March 1, 2003 – December 31, 2003

April 2004

[1] Principal Investigator, Professor of Mechanical Engineering and Director of GDTL
[2] Graduate Student

ABSTRACT

The dynamics of large-scale turbulence structures within a high Reynolds number, ideally expanded Mach 1.3 jet were investigated during both the periods of production of strong acoustic radiation and extended periods of relative quiet that lacked such acoustic radiation. These results were acquired through a unique experiment where the sources of large amplitude sound waves were estimated with a three-dimensional microphone array and the flow field was simultaneously visualized on two orthogonal planes. The images from one of the planes were taken at a 167 kHz rate. Proper Orthogonal Decomposition (POD) was employed to create a basis of the size and distribution of large-scale structures within the two planes. These POD modes were then used to objectively determine the differences in the jet structure during noise generation and periods lacking significant noise generation. The results show that the flow during the periods of relative quiet cases is dominated by the lower order POD modes that consist of relatively large turbulence structures while it is dominated by higher order POD modes that capture the dynamic interplay of the large-scale structures during noise generation periods. For approximately one convective time scale prior to the moment of noise emission, a series of large-scale structures forms and disintegrates within the mixing layer and in the process a large amount of ambient fluid is entrained into the core of the jet. For the first time, these results show how the dynamic interplay of large-scale turbulence structures generates acoustic radiation within a high Reynolds number jet.

Table of Contents

INTRODUCTION

The fundamental relationship between the dynamics of turbulence and the generation of sound has eluded the efforts of researchers for well over 50 years. The first treatment of the problem was presented by Lighthill [1952, 1954] in his seminal work that established a relationship between the average sound pressure and the n^{th} power of the jet's exit velocity. For low to moderate-speed jets, n is 8, while for high-speed jets n approaches 3 [Lilley 1991]. By utilizing larger by-pass ratio engines, the effective velocity of the exhaust has been significantly reduced, efficiency has improved and the noise levels have dropped. However, additional reductions in noise levels are required, and increasing the by-pass ratio further might cause problems in aircraft design, decreased fuel efficiency and increased fan noise [Neise and Enghardt 2003]. In spite of much effort, the mechanisms that are responsible for the generation of jet noise are still not well understood. The goal of this research effort is to gain a better understanding of the relationship between the dynamics of large-scale structures in the jet and the far-field radiated noise in high subsonic and ideally expanded supersonic jets.

With the pioneering works of Crow and Champagne [1971] and Brown and Roshko [1974] that established the existence of large coherent structures in free shear layers, new thinking about turbulence generated noise flourished. One of these aspects is a focus on the generation of sound by dynamics of large-scale structures. In moderate to high Reynolds number jets, the noise generated by the large structures preferentially radiate at shallow angles ($\theta \sim 30°$) over a relatively narrow distribution of frequencies ($St_D \sim 0.1$ to 0.5) [Tam 1991, Simonich et al. 2001, Hileman and Samimy 2001]. The preferential radiation at shallow angles is due to the convection of the large structures with respect to the ambient [Ffowcs Williams 1963, Lilley 1991]. At other observation angles ($\theta \sim 90°$), the acoustic far-field spectrum is broadband and relatively flat. The radiation due to the dynamics of large-scale structures is the focus of this work ($\theta \sim 30°$).

Much work has been conducted with the goal of obtaining a relationship between the dynamics of large structures that are present within a shear layer of high-speed jets and the generation of acoustic radiation. Such information would tremendously aid in the modeling of turbulence mixing noise. The majority of the turbulent mixing noise that originates from large structure dynamics emanates from a region that surrounds the end of the potential core. This determination has been made with an examination of the far-field acoustic radiation with a variety of microphone arrays [e.g., Fisher et al. 1977, Venkatesh et al. 2003] as well as an examination of the near-field pressure [Tam 1991]. One has to understand the dynamics of the large structures to understand how they generate noise because a time-dependent phenomenon is required for the generation of sound [Lighthill 1952, 1954, Crighton 1975, Lilley 1991]. Many works have confirmed that an unsteady source is necessary for sound generation within high Reynolds number jets [e.g., Sarohia and Massier 1977, Morrison and McLaughlin 1979, Stromberg et al. 1980, Freund 2001].

This work is a continuation of the work presented in Hileman & Samimy [2001] and Hileman et al. [2002] where attempts were made to connect the dynamics of large coherent structures within a high Reynolds number, ideally expanded Mach 1.3 jet mixing layer to large amplitude sound 'waves' that reach a microphone array in the acoustic far-field at shallow angles ($\theta \sim 30°$). Simultaneous point measurements of the flow and acoustic fields have been conducted in the

past [Lee and Ribner 1972, Siddon 1973, Schaffar 1979, Panda and Seasholtz 2002], but for jets that lack Mach wave radiation, these experiments often show a lack of coherence between the two measurements. This and the previous works [Hileman and Samimy 2001, Hileman et al. 2002] are the first to use a microphone array with simultaneous flow measurements. In addition to this unique aspect, these works represent the first attempts to find differences between the dynamics of the large structures during periods when sound is being created and periods that lack such acoustic radiation. By understanding the differences in the large structure dynamics between these two different 'states' of the jet, one will gain an understanding of what structure dynamics are important to the creation of acoustic energy. In Hileman and Samimy [2001], the acquisition of the acoustic field was accomplished with a dual microphone array for noise source location and the flow was captured via dual-pulse flow visualization. In Hileman et al. [2002], this technique was greatly improved upon with a four-microphone inline array and the use of a temporally resolved flow visualization system. In this work, a 3-D microphone array was used to locate the noise origins while two flow visualization systems captured the dynamics of the jet. The two visualization systems simultaneously captured the temporal evolution of the jet in a streamwise plane between 6 and 12 x/D as well as a single image in a cross-stream plane at 9 x/D. These locations were chosen as they are within the main noise emitting region of the Mach 1.3 jet under study. These results are being analyzed with the Proper Orthogonal Decomposition (POD) technique to capture the essential differences in the dynamics of the flow between noise generation periods and periods lacking significant noise emission. The examination shows how the dynamics of the large structures are different during noise generation and periods lacking significant sound production.

EXPERIMENTAL FACILITY AND TECHNIQUES

All of the experiments were conducted in the optically accessed anechoic chamber of the Gas Dynamics and Turbulence Laboratory (GDTL) of The Ohio State University.

Jet Facility and Anechoic Chamber

This facility is equipped for the measurement of jet flows via optical diagnostics in a fully anechoic environment (Fig. 1). The inner dimensions of the chamber, from wedge tip to wedge tip, are 3.12 meters in width and length, and 2.69 meters in height. Additional details of the anechoic chamber as well as its validation can be found in Kerechanin et al. [2001]. Details of the jet facility can be found in Hileman et al. [2002] and Hileman [2004]. The jet nozzle had a 25.4 cm (1 inch) exit diameter and was designed using the method of characteristics for a Mach 1.3 flow. It was operated at the ideally expanded pressure. The actual Mach number of the jet was 1.28 and it had a Reynolds number of 1.08×10^6. The reasons for using an unheated, Mach 1.3 jet were to achieve a convective Mach number match to a heated Mach 0.9 jet typical of a commercial jet engine (with a stagnation temperature of 810°K and M_c of 0.55) and to facilitate flow visualization, as will be further discussed later.

Simultaneous Data Set

Two sets of measurements were acquired simultaneously in this work: acoustic source localization in three-dimensions and flow visualization of two planes within the flow. Figure 1 shows a schematic of the experimental set up as viewed from above. A rather large amount of simultaneous data consisting of 19,750 sets of flow images with simultaneous microphone array measurements were acquired over the course of four days. Each data set consisted of a single flow image in the cross-stream, seventeen temporally resolved flow images of the streamwise plane (at 167 kHz rate), and 8192 data points (8.192 ms of data) from the eight microphones of the 3-D array. The data set was approximately 70 GB. Such a large data set was acquired to ensure a large number of images were obtained during noise generation periods. The laser systems and one of the cameras were located outside of the anechoic chamber, while another camera was inside the chamber perpendicular to the streamwise laser sheet. Apparent noise source origins were computed in four-dimensional time-space for every far-field, shallow-angle (30° from the jet axis) acoustic event with amplitude in excess of 1.5 times the standard deviation using the 3-D microphone array. Details of how the timing between the flow and acoustic data was established are given in Hileman and Samimy [2001] and Hileman [2004].

3-D Microphone Array

The purpose of this work is to explore the relation between the *dynamics* of large turbulence structures in the jet and the emission of sound from the jet; hence a temporal domain analysis was used, where the origin of individual sound events was determined. The array works by measuring the phase lag of individual sound events between microphones in space. With this phase lag information and the geometry of the array, a sound origin is determined for every acoustic event with amplitude exceeding 1.5σ (standard deviation of the sound pressure). The array is placed at a 30° location as this is the location of maximum sound emission [Hileman and

Samimy 2001] and this radiation is associated with large turbulence structures. The present 3-D microphone array/analysis algorithm is a third-generation design that measures the phase difference between an individual acoustic peak being recorded by various microphones in space. The microphone array has a total of eight microphones: six azimuthally distributed to determine the origin in the cross-stream plane and two sets of inline microphones to determine the origin along the jet axis (streamwise direction). A plasma arc was used to test the 3-D microphone array's ability to locate noise sources of varying frequency content. An acoustic tone was created by the arc that could be precisely controlled between a few hundred Hertz and 20 kHz. A repetitively pulsed plasma arc and a small fluidic device were used to evaluate the microphone array. The plasma arc approximated a point source to test the frequency response while the fluidic device was modified to produce resonant (2.1 or 3.4 kHz tones) as well as broadband (central frequency of 7 kHz) acoustic radiation. The microphone array accurately located the source region of the fluidic device as well as the plasma arc when it was producing acoustic frequencies under 10 kHz. For this reason, the acoustic data was low pass filtered at 10 kHz using a fifth order Chebyshev type I digital filter. Further details of the microphone array can be found in Hileman et al. [2004] and Hileman [2004].

Flow Visualization

Two laser sheets were used to simultaneously visualize two orthogonal planes of the jet. The orientations for the two sheets are shown in the schematic of Figure 2 Condensation of moisture from the ambient air entrained into the jet mixing-layer was used to visualize the flow and to track the evolution of large-scale turbulence structures within the jet. One laser sheet was placed normal to the jet flow at a streamwise location of 9 x/D (hereafter referred to as the cross-stream sheet). This sheet was created with a Spectra Physics Pro-250 Nd:YAG laser while the flow images were captured using a Princeton Instruments ICCD camera that had a resolution of 576 by 384. The streamwise laser sheet was visualized in real-time over periods of 96 μs at a rate of 167 kHz (6 μs separation). This temporally resolved flow visualization was made possible by a pulse burst laser / high frame rate camera system. The pulse burst laser was built in-house and it operates at 532 nm with about 15 mJ of power per pulse. The number of laser pulses was set at 17 with 6 μsec separation between pulses. A Dalsa model 64K1M camera was used to acquire the images. The cross-stream sheet was acquired simultaneously with the seventeenth flow image of the streamwise, temporally-resolved set of images. Further details on the pulse burst laser / flow visualization technique can be found in Thurow et al., [2002, 2003].

Proper Orthogonal Decomposition (POD)

POD has been used extensively to identify the most energetic structures/modes in jet flows [e.g., Ukeiley and Seiner 1998, Citriniti and George 2000, Caraballo et al. 2003]. The POD technique was introduced to the turbulence community as an objective means of extracting coherent structures from turbulence data by Lumley [1967] and it is known as the Karhunen-Loeve technique in other areas of study. It works by mathematically decomposing a flow field into a set of eigenmodes that capture the flow's most energetic features. In a sense, the first mode captures the most common deviation from the mean while the second captures the most common deviation from the first and so on. These eigenmodes yield a distribution in size and space of the POD modes (representing coherent structures in some sense) within the flow and multiple modes are generally required to gain a proper representation of the large structures. The field used to

create the POD modes can be projected onto the modes to calculate a set of weighting factors, which in turn can be used to reconstruct the flow from a select number of POD modes. These weighting factors are often referred to as temporal coefficients since they can also be used to determine the relative importance of each mode over a time series of the field.

The POD analysis of this study uses image intensity fluctuations as the working variable, and the technique is optimized for intensity variance. The modes are ordered based upon the percent of the total captured intensity variance. The methodology used here relies on the snapshot method of Sirovich [1987], and it follows that of Caraballo et al. [2003] to compute the eigenmodes. The snapshot method was designed for the analysis of highly spatially resolved data, and it requires a sufficiently large number of uncorrelated realizations of the image field (both are qualities of the flow visualization images employed here). Others have used the snapshot POD method to extract information from images of human faces [Sirovich and Kirby 1987, Sirovich and Everson 1992]. Additional details on how POD was used in this study can be found in Hileman [2004].

Since the quantity being analyzed with POD is image visualization intensity, additional considerations must be made for image processing. The image intensity of any flow visualization image relies on three things: the seed particles that are marking the flow, the intensity of the light that is illuminating the particles, and the camera that is capturing the images. In the flow visualizations used in this work, the dew point changed over the course of image acquisition and the laser power varied. Both of these will affect the flow visualization quality as will be discussed later. Because of this, it was deemed unacceptable to allow fluctuations in intensity (other than a simple on-off binary difference) into the POD calculations. The binary images show a region as being mixed (sufficient condensation present) or not mixed (insufficient condensation). This topic was discussed at length in Hileman [2004].

EXPERIMENTAL RESULTS

Acoustic Data

The 3-D microphone array was used to locate the sources for all large amplitude events in excess of 1.5σ (σ is the standard deviation of the sound pressure) for 4.4 ms of data within each of the 19,750 sets of acoustic data. This yields a total of 86.7 s of data that was analyzed. This can be compared to the 5 s of data that was taken before this set of experiments and was presented in Hileman et al. [2004]. Out of the 86.7 s of data, there were 222,907 large amplitude events examined for their respective noise sources. The mean values for the three spatial coordinates $[x_s, y_s, z_s]$ are [9.1, 0.0, 0.4] D with standard deviations of [2.2, 0.3, 0.4] D. The non-zero mean z source location was due to misalignment of the array's centerline with that of the jet and this value is still small compared with the diameter of the array (52.0D). The mean values of y_s and z_s were subtracted from the individual noise sources prior to compilation into probability distributions.

The probability distributions for the spatial origin of the noise sources are given in Figure 3. The streamwise distribution (shown in *a*) was created with a bin size of 0.5D while the cross-stream distribution (shown in *b*) was created with a bin size of 0.125D. The streamwise distribution shows that the vast majority (90%) of the noise sources originated between 5.5 and 12.5 x/D while the cross-stream distribution is round as expected. Combining the two measurements, one realizes the region of noise generation is an ellipsoid that is centered on the jet centerline at 9 x/D. This should be expected since the mixing region spans the width of the jet past the end of the potential core.

All of the large amplitude events that were analyzed for their spatial origin were also examined for their frequency content. With this information, the frequency of the large amplitude events could be plotted against the origin of the events in the form of probability distributions. The frequency content of the large amplitude events was determined with the use of the Matlab® function 'fminsearch', which finds the minimum of a scalar function of several variables starting with some initial estimate using an unconstrained nonlinear optimization. The function used for optimization is the Mexican hat wavelet, which has a similar shape to a waveform created from an average of the large amplitude acoustic events [Hileman et al. 2002]. The probability distribution of Strouhal number as a function of streamwise noise source location was computed using a bin size of 0.5 x/D by 0.05 St_D. This distribution, as well as another showing the distribution of normalized sound pressure as a function of streamwise location, is given in Figure 3 (*c*) and (*d*). The binning on the normalized sound pressure distribution is 0.5 x/D by 0.05σ. The Strouhal number – source location distribution (*c*) shows a dependence of Strouhal number on the streamwise location with higher frequencies originating closer to the jet nozzle exit. This is a common trait to noise source location distributions. The line within the figure shows a fit to the subsonic jet noise source data of Venkatesh et al. [2003], which spanned a range of Mach numbers between 0.5 and 0.9 for both heated and unheated jets. They analyzed a range of frequencies from a St_D of 0.2 to 10. As shown, the current data set matches the trend of the Venkatesh et al. curve quite well. The magnitude – source location distribution (*d*) shows that the largest amplitude events are being created between 8 and 10 x/D.

Flow Visualization

To maximize the likelihood of capturing flow images during the creation of large amplitude noise events, the two orthogonal laser sheets were centered on the mean of the noise source distribution as shown in Figure 2. A typical instantaneous cross-stream image is shown in Figure 4. This figure gives both the raw image showing the entire intensity range (*a*) as well as the image converted to binary (*b*). An average of many of these binary images is round with a decreased intensity towards the center. Figure 5 shows a typical image from a streamwise image set (one of the seventeen temporally-resolved images in a set is shown). The first image (*a*) has been modified by the removal of a horizontal line at 9 x/D (caused by the cross-stream laser sheet), digital filtering, and a normalization procedure that brought the intensities of all of the columns to a maximum value of one. The second (*b*) shows the flow visualization image after conversion to binary. Due to image quality issues with the streamwise data set, only 10,750 sets of streamwise, temporally-resolved images were used.

POD Modes

The first 24 POD modes were computed for the cross-stream flow visualization images using the image intensity fluctuation from the mean. The modes were constructed from 2000 of the 19,750 images. An emphasis must be placed on the fact that the images that were used for POD were converted to binary before modal analysis. Another important note is that the relative sign of the structures is not important among the POD modes, only the relation of the signs within an individual mode matters. The POD modes are presented in Figure 7 with the percent of the total intensity variance captured in each mode given in the figure. The grayscale of the images shows positive (white) and negative (black) intensity fluctuations from the mean. The convergence of these modal shapes was examined in Hileman [2004] and a few of the higher order modes changed shape between set sizes of 1500 and 2000. Even though an increase in set size might change some of the modes slightly, this set of POD modes can be thought of as a basis that captures all of the large structures and their spatial distributions within the flow images. The first 11 modes reflect what is occurring around the periphery of the mixing layer and these modes mostly occur in pairs, i.e. modes 1 and 2 have two alternating-sign structures, modes 3 and 4 have four such structures, modes 5 and 7 consist of three structures, and modes 8 and 9 consist of eight structures. The higher order modes (12 through 24) consist of structures that span the entire mixing layer. Modes 14 through 18 have a clearly defined structure at the jet center, while modes 22 and 23 have a pair of such structures. Mode 15 is unique in that it has a dominant center structure. Modes 18 and 21 also have alternating sign structures (12 structures) around the periphery of the jet, but there is also a structure at the jet center. A few of the higher order modes (19, 20 and 24) are quite complex and bare similarity to the cut-and-connect torroidal structure described by Hussain [1986]. Even though there are a large number of modes computed here, they only comprise 40% of the total intensity variance. For a POD problem such as this (involving image intensity), one must have a very large number of modes to capture all of the intensity variance. However, the distribution of the large structures should be captured as evidenced by the decreasing size of the structures that are within higher modes.

The first 16 streamwise POD modes were computed from the sixth image (of a 17-image set) of 2000 of the 10,750 temporally resolved flow visualization image sets. These modes are presented in Figure 8. The POD decomposition was applied to the region between 7 and 11 x/D to emphasize the area surrounding the maximum noise source concentration. As was the case for

the cross-stream modes, the intensity variance had reached convergence with this image set size, but, the addition of more images to the set would likely lead to some small changes in the higher modal shapes [Hileman 2004]. There is a distinct order present in the streamwise modes. The first four modes depict large oval-shaped structures that span large streamwise distances and are located within the outer region of the mixing layer. In modes 1 and 2, these structures have a clearly asymmetric arrangement while mode 3 has a symmetric arrangement. Modes 5 and higher have structure within the inner as well as outer regions of the jet. In modes 5 and 8 the large structures are clearly asymmetric while modes 9 and 12 have structures that are symmetric about the jet centerline. Modes 4 and 6 lack symmetry, which could be an artifact of the flow imaging procedure, i.e. it is quite difficult to achieve exact symmetry in an experimental setup. The tremendous symmetry that is present within these modes is really impressive when one considers that the POD modes were created from flow visualization image intensity and not a quantitative measurement such as velocity, density or pressure. Many of the higher modes (8-16) have smaller structures within the outer regions of the jet and these are tilted, which is a common trait of large-scale structures that are within a shear flow. Mode 15 of the cross-stream POD consisted of a single structure at the jet centerline (Figure 7), which is similar to mode 11 of the streamwise POD. As will be presented and discussed shortly, dynamics of this POD mode apparently play a large role in the noise generation process.

NG and RQ Selection Criteria

This work focuses on two 'states' of the Mach 1.3 jet. One of these states corresponds to noise production within the jet (noise generation, NG) while the other corresponds to a relative lack of noise production (prolonged period of relative quiet, RQ). The flow image sets used in the reconstruction of these two states will be selected based on noise source locations from the microphone array. The NG sets (one for the cross-stream and one for the streamwise images) were chosen based on large amplitude acoustic events that were larger than 2.0σ. The noise source distributions of earlier sections used a 1.5σ criterion. For both laser sheets, determination of which images will be included in the NG data sets relies on knowledge of when and where the large amplitude events originated within the jet (four-dimensional, space-time, noise source localization). The RQ sets (one for the cross-stream and one for the streamwise images) will rely simply on the retarded time for an acoustic wave and the duration of the period of relative quiet.

In order for an image to be selected for the NG data set, there must be an associated large amplitude noise event that reached the top front microphone of the array and this noise event had to meet criteria in space and time. A similar peak was also required to reach the bottom front microphone of the array within a small time interval. For a streamwise image to be included in the NG data set, the large amplitude event source needed to be between 7 and 11 x/D. To be included within the cross-stream NG data set, the source of the large amplitude event needed to be between 8 and 10 x/D, which is within 1 x/D of the illuminated plane. For both sheets, the z-location of the noise source for the large amplitude event was required to be above the jet centerline as determined by two measurements: 1) the noise source location calculation and 2) the phase lag measurement between the top front and bottom front microphones. The reason for the scrutiny on the z-location criterion was to minimize the effect of refraction on the noise source location (NSL) procedure, which for these measurements was based on measurements from the top half of the microphone array (see Hileman [2004] for reasoning and methodology behind this top-half approach). The time the large amplitude event was created relative to the

flow illumination by the laser sheet was also determined. This time lag criterion was analyzed differently for the cross-stream and streamwise images as will be discussed shortly. Finally, as mentioned at the start of this paragraph, the bottom front microphone of the array was required to record a large amplitude event having the same sign within 0.1 ms of the top front microphone recording the event. This ensured the sound wave was radiated uniformly over all azimuthal directions, and the event was not an anomaly recorded by the top front microphone. This last requirement certainly eliminates some good large amplitude noise source data since refraction will deflect some acoustic radiation away from the bottom set of microphones. However, such refraction increases the uncertainty in the computation of the origin of the large amplitude event. By making this requirement, though, there is a guarantee that the captured structure dynamics generate acoustic energy that travels uniformly in all azimuthal direction.

The time lag between flow illumination and acoustic wave creation was used as the final criterion for image selection for the NG data sets and it was examined differently for the cross-stream and streamwise flow visualization images. For the cross-stream, the time lag between the flow illumination and the estimated emission of the large amplitude event had to be under 0.5 convective time scales (t^*u_c/D). This yielded a set of 200 flow visualization images that would be analyzed for their noise generation characteristics. The streamwise images were acquired in sets of seventeen images with a separation of 6 μs. The seventeenth image was not used due to contamination by the simultaneously visualized cross-stream laser sheet. Due to the large number of images that were captured at a known time relative to the estimated moment of noise generation, the temporal aspect of noise generation was examined with this data set. To understand how this was done, consider a case where the moment of noise generation coincides with the sixteenth flow image, then there are fifteen time-correlated images that come before the moment of noise generation. If the noise generation moment coincides with the first image, then one has fifteen images showing the flow development afterward. By extending this concept to large times before and after the moment of noise generation (i.e., one can collect all images that were acquired a set time before or after the moment of noise emission), a crudely phase-locked series of images can be ensemble averaged to create a depiction of the average process of noise generation. There were 1846 large amplitude events meeting the criteria outlined previously that were created over a 1 ms span including the moment of noise generation. There were 16 streamwise images corresponding to each of these large amplitude events. By phase alignment of the images relative to the moment of noise emission (estimated creation time for the large amplitude event), a time series was created showing the average large structure dynamics that are responsible for the generation of acoustic energy. This series of pseudo phase-locked data consists of 134 time steps separated by 6 μs (402 μs before and after the estimated moment of peak acoustic energy creation), and each time step was comprised of approximately 180 images. Two and a half convective time scales of data will be presented here while more of the data can be found in Hileman [2004].

The RQ data sets were selected based upon a lack of noise generation above 1.5σ over a minimum duration with consideration of the retarded time for sound wave propagation in the jet. A sound wave required 3.32 ms to travel from the center of the noise source distribution to the top front microphone of the array. This retarded time combined with the delay between the start of acoustic data acquisition and the flow illumination (0.48 ms) yields a time of 3.8 ms, which is the required center for the relative quiet period. For both flow visualization RQ sets, the period of relative quiet requirement was a width of at least 0.5 ms (~5 convective time scales) with a

center of 3.8 ms. The 200 cross-stream data sets that had the longest periods of relative quiet were used and the shortest such period was ~ 13 convective time scales. The streamwise RQ data set was not phase-locked since there is no phase-defining event. Instead, the 180 longest periods of relative quiet were chosen to define the RQ state; thus, there are simply 180 sets of 16 images that can be used to describe the RQ state. The lengths of relative quiet (average value for the two front inline microphones of the array) in the streamwise RQ data set were at least 1.0 ms (~11 convective time scales) with a maximum of 2.7 ms (~29 convective time scales).

The magnitude of the normalized sound pressure data for the streamwise NG and RQ data sets are presented in Figure 8. The average NG acoustic data was created from 2 ms surrounding the 1846 acoustic events, while that of the RQ was created from the 180 sets of acoustic data. The NG data set has a large amplitude peak while the RQ data set has a distinct 'well' of reduced sound pressure. The 0.5 ms range that was required to be considered a relative quiet period is clearly defined in the figure between 3.6 and 4.0 ms. The gradual increase on either side shows the varied lengths of relative quiet among the RQ acoustic signatures.

Image Reconstruction

The POD modes were used as a basis that describes the shape, size, and spatial distribution of the large structures within the jet. With these modes and a judicious selection of weightings (time coefficients), one could reconstruct a typical image of the jet to a reasonable approximation. One could also use them to look for differences between the NG and RQ image sets. The POD time coefficients were determined for every image within these two sets along with a randomly selected image set. For the cross-stream cases, 24 time coefficients were determined for each image since there were 24 computed POD modes, while the streamwise images had 16 time coefficients for the 16 POD modes. For the POD modes, the positive or negative sign of the structure only has significance within individual modes (i.e., to determine asymmetry vs. symmetry of a mode). The sign of one mode is irrelevant to another mode. However, in modal reconstructions, the sign is quite important. The sign of a reconstructed image shows the deviation from the image mean. Lighter regions have greater than average intensity (increased entrainment and mixing, i.e. presence of large structures) while darker regions have lower than average intensity (corresponds to a lack of mixing and large structures). These time coefficients could then be averaged across the entire data set to yield a representative coefficient for each POD mode.

The average time coefficients may not mean much since the structure of the jet is constructed from a combination of multiple POD modes. Instead of comparing the average time coefficient for each mode individually, they will be combined to reconstruct the jet. The procedure is straightforward: the average time coefficient is used as a weighting factor for each mode and the weighted modes are combined to reconstruct the jet's structure. The values of the individual modes can be found in Hileman [2004]. The cross-stream reconstructed images are shown in Figure 9. All of these reconstructed images are plotted on the same intensity contours. The first row of images shows the reconstructed images using all 24 modes. The RQ reconstructed image is dominated by relatively large structures around the periphery of the jet. This is in contrast to the NG reconstructed image, which consists of many smaller structures that span the entire cross-section of the jet. The random reconstructed image seems to be a combination of the NG and RQ, as one would expect. There is a clear difference between the RQ and NG states based on both structure size and the radial location of these structures. The second row of Figure 9 shows

the reconstructed jet using the first 11 modes, which were dominated by relatively large structures that were on the periphery of the jet. The RQ reconstructed image (using modes 1-11) shows structures similar to those constructed using mode 1-24, indicating these lower order modes dominate during relative quiet periods. This is a distinct contrast to the average NG reconstructed image, which lacks structure; in other words, the lower order modes (modes 1-11) were not important while the jet was creating noise (NG state), but they dominated during periods of relative quiet (RQ state). The third row of the figure shows the reconstructed images using modes 11 through 24, which consisted of smaller structures that spanned the entire jet cross-section. The RQ reconstructed image has alternating positive and negative fluctuating structures (negative on the outside) with a lack of any structure at the jet's center. The NG reconstructed image also has alternating positive and negative fluctuating structures on the jet's periphery, but the positive fluctuations are now on the outer portions and there is a strong, positive fluctuation at the jet's center. Thus, during noise generation, the jet was dominated by many relatively small alternating structures (these are also considered large-scale structures) that surround a large structure at the jet centerline. This large structure is absent from reconstructed images of periods of relative quiet.

One must remember that all of the structure scales that are being observed in these reconstructed images fall into the large-structure category. None of them could be classified as small-scale since they are on the order of magnitude of the jet nozzle exit, D. Truly small-scale structures are many orders of magnitude smaller than any observed in the POD reconstructed images of this high Reynolds number ($\sim 10^6$) jet.

As discussed in the last section, the reconstructed images of the streamwise NG and RQ data sets were dealt with differently than those of the cross-stream since they have temporal resolution allowing for the analysis of the large-scale structure dynamics. The sixteen streamwise POD modes were used to reconstruct 40 time steps (234 μs or ~2.5 convective time scales) that are crudely phase-locked to the moment of noise generation for the NG data set and a series of 16 time steps (90 μs) of the development during RQ were reconstructed. To facilitate the analysis, the two sets of images were reconstructed using modes that dominate the outer part of the jet (modes 1-4) and those spanning the entire cross-section of the jet (modes 5-16). The four-mode (1-4) reconstructed temporally resolved image sets are given in Figure 10 (both NG and RQ). The four-mode, reconstructed RQ image set has large structures possessing strong, positive fluctuations while the four-mode reconstructed NG image set has spatially large, but negative fluctuation structures for 40 μs on either side of the estimated time of noise emission (0 μs). At the moment of noise emission, there is actually a lack of any structures (positive or negative), which is in agreement with the reconstructed image of the cross-stream plane using the outer POD modes (see reconstructed NG images using modes 1 to 11 of Figure 9). The streamwise, reconstructed RQ image set also matches the cross-stream, RQ reconstructed RQ image with larger structures dominating. The sign of the structures within the streamwise reconstructed RQ image set match those of the cross-stream reconstructed RQ image. In both cases, a positive (white) region is located above the jet centerline while a negative (black) region is below. This result becomes even more impressive if one considers that the cross-stream and streamwise reconstructed images were created from flow visualization images taken with two independent and quite different laser-camera systems. When the streamwise reconstructed RQ and NG images are created from the higher order modes (5-16), the results are astounding. The RQ and NG image sets that were reconstructed using modes 5-16 are given in Figure 11. The

reconstructed RQ image set has a negative fluctuation region at its center while the reconstructed NG image set has a region with positive fluctuation at the same location for times between -20μs and +80μs. Before the noise emission time of 0μs (-100μs to -30μs), the top half of the mixing layer has a series of alternating sign structures. Immediately before the moment of noise emission (-30μs to 0μs), this alternating series of structures is replaced by a single positive structure that lies on the jet centerline and this dominates the reconstructed images thereafter. The formation and disintegration of the alternating, large structures within the top half of the mixing layer bares an uncanny similarity to a process hypothesized in Morrison and McLaughlin [1979]. They conjectured the majority of the noise within a low Reynolds number (3700), Mach 1.4 jet is due to the rapid decay (disintegration) of instability waves within the jet, and this disintegration involves a "relatively violent fluid dynamic action." The temporally resolved image set shown in Figure 11 is the first to capture this noise generating 'fluid dynamic action' within a jet.

Apparently, the positive intensity fluctuation region at the center of the jet is a key aspect of noise generation since it is a dominant feature during noise generation within both the cross-stream and streamwise directions. A positive intensity fluctuation at the centerline region is indicative of interaction between the two sides of the jet's mixing layer; while a negative fluctuations region shows that such interaction is not present (there is a clear separation of the sides of the jet). Ahead of the time of noise emission (-100 μs to -40 μs), the large robust structures along the top of the jet entrain large amounts of ambient air into the jet. Apparently, some form of cross-mixing layer interaction is a key aspect of the jet's structure during periods of noise generation, and this is not present during the prolonged periods of relative quiet. The periods of relative quiet also had a series of robust structures, but it did not have entrainment of the ambient air into the centerline. This observation is in agreement with the subjective interpretations of the simultaneous data presented in Hileman and Samimy [2001] and Hileman et al. [2002]. Another interesting difference between the two states (NG versus RQ) is the sizes of the structures that dominate. The RQ state has large structures with less interaction than the NG state, which is dominated by interactions of relatively small structures. One has to remember, though, that these modes are fluctuations from the mean image. Hence, the last observation likely shows that during noise generation there are more interactions between dynamic and relatively smaller structures than the larger but benign structures that are prevalent during periods of relative quiet.

SUMMARY AND CONCLUSIONS

Through a unique experiment, the dynamics of large-scale turbulence structures within a high Reynolds number, ideally expanded Mach 1.3 jet were investigated during both the production of strong acoustic radiation and extended periods of relative quiet. The results consisted of three-dimensional noise source locations and flow visualization images from two orthogonal planes. POD was used to create modes for the two planes and these were used to reconstruct images that were acquired during noise generation and periods lacking significant noise generation. For the first time, these results show how the dynamic interplay of large-scale turbulence structures generates acoustic radiation within a high Reynolds number jet.

There is a distinct difference in the jet's structure during the time preceding and following noise generation as compared to the structure during periods that lack noise generation. This difference was observed through a novel approach where the origins of large amplitude sound events were correlated to simultaneously acquired temporally resolved flow images. To ensure statistical viability of the results, a large set of simultaneous flow and acoustic data was acquired that consisted of 19,750 sets of acoustic data from the 3-D microphone array and flow images in two orthogonal planes. Both image planes were centered on the region of maximum noise source concentration (9 x/D), and the images were decomposed using POD to extract a basis of the relative size and position of the large-scale structures. The symmetry of the POD modes was remarkable as they were easily grouped into those that emphasize large-scale structure positions within just the outer portion of the mixing layer and those that spanned the cross-section of the mixing layer.

Images of the flow during noise emission (NG) or periods of relative quiet (RQ) were identified, based on analysis of the acoustic data from the 3-D microphone array. The dramatic difference in the acoustics waveforms of these sets was shown in Figure 8. The POD modes were used to reconstruct the cross-stream and streamwise images within the NG and RQ data sets. These reconstructed images show the dramatic differences between the NG and RQ states of the jet.

In the introduction, some works were presented that discussed what occurs within the region of sound generation of a high-speed jet. Among these, Freund [2001] pointed out that the Lighthill acoustic sources within a low Reynolds number, Mach 0.9 jet changed dramatically in space and time near the end of the potential core and this is the region with the maximum acoustic radiation. The dominant noise production mechanism speculated upon by Morrison and McLaughlin [1979] was the rapid growth, saturation, and decay of instability waves near the end of the potential core. They made this conclusion based upon hot-wire measurements within a low Reynolds number (3700), Mach 1.4 jet. Immediately downstream of the end of the potential core (where the acoustic waves of their jet originated), they found the coherence of the velocity fluctuations from hot-wire measurements decreased dramatically. Based on these observations, they conjectured that the majority of the noise was due to the rapid decay (disintegration) of the instability waves. A comparison of the mean noise source region to statistical flow images of the Mach 1.3 jet examined in this work showed the majority of the noise was coming from a region dominated by the interaction of the two sides of the mixing layer (potential core end). This is in agreement with the low Reynolds number works just discussed. The results presented in this work show for the first time the nature of the large-scale structures and their dynamics that are responsible for noise generation within a high speed jet.

Noise generation within the high Reynolds number, Mach 1.3 jet was dominated by a set of relatively small structures (but still on the order of a fraction of nozzle exit diameter) that entrained fluid into its center. These structures were observed in a 9 x/D cross-stream plane (Figure 9) and a crudely phase-locked series of images in the streamwise plane (Figures 10 and 11). These organized series of structures persisted from -100 μs to -24 μs (time relative to noise emission) before abruptly disintegrating shortly before the moment of sound emission. Prior to their breakdown, the series of structures tilted dramatically between -90 and -36 μs. In their place, a positive intensity fluctuation persisted at the jet centerline between 7 and 9 x/D; it had little activity with the outer regions of the jet. This positive fluctuation shows much fluid has been entrained to the jet centerline. The large-scale structure interaction might take the form of the 'tilt-stretch-tear-pair' observed by Thurow et al. [2003] since those images were taken of the same jet that is being examined here. Since it is unlikely that only one mechanism is responsible for the creation of noise, multiple mechanisms are likely being smeared within these images.

As to the question of how to make jet engines quieter, the reconstructed relatively quiet images have a well defined unmixed core as shown by the negative intensity fluctuations at the jet centerline. This is opposite to the reconstructed NG images. Although not shown here, the unmixed cores of the ten best RQ image sets move in a wave-like motion with large structures surrounding it [Hileman 2004]. This rotation of the unmixed core of the jet was captured by Thurow et al. [2003] in a time-resolved flow movie of this jet at a cross-stream location of 6 x/D. Based on these results, noise reduction might be achieved by promoting the growth of large-scale structures that rotate around the jet centerline (a helical mode) where the unmixed, potential core of the jet is stretched as far as possible. Such a jet would inhibit the interaction of the large structures by maintaining a buffer between them, and the energy that is contained within them would be dissipated by their gradual disintegration instead of the abrupt changes observed in Figures 10 and 11. Of course, this noise reduction scheme is only a conjecture at this point.

ACKNOWLEDGMENTS

The support of this work by the Air Force Office of Scientific Research is very much appreciated. We acknowledge the help of many colleagues at GDTL, including Jeff Kastner, and Walter Lempert. The last three authors would like to thank the Ohio Space Grant Consortium, DAGSI and the Department of Defense (NDSEG), respectively, for their doctoral fellowships.

REFERENCES

Brown, G. L. and Roshko, A., (1974) "On Density Effects and Large Structure in Turbulent Mixing layers," *J. Fluid Mechanics*, Vol. 64, pp. 715-816.

Caraballo, E., Samimy, M., Scott, J., Narayanan, S. and DeBonis, J., (2003) " Application of Proper Orthogonal Decomposition to a Supersonic Axisymmetric Jet," *AIAA J.*, Vol. 41, No. 5, pp. 866-877.

Citriniti, J. and George, W., (2000) "Reconstruction of the Global Velocity Field in the Axisymmetric Mixing layer Utilizing the Proper Orthogonal Decomposition," *J. Fluid Mechanics*, Vol. 418, pp. 137-166.

Crighton, D.G., (1975) "Basic Principles of Aerodynamics Noise Generation," *Prog. Aerospace Sciences*, Vol. 16, pp. 31-96.

Crow, S. C. and Champagne, F. H., (1971) "Orderly Structure in Jet Turbulence," *J. Fluid Mechanics*, Vol. 48, Pt. 3, pp. 547-591.

Ffowcs-Williams, J.E., (1963) "The Noise from Turbulence Convected at High Speed," *Philos. Trans. Royal Soc. London*, Ser. A, Vol. 255, No. 1061, pp. 469-503.

Freund, J., (2001) "Noise sources in a low-Reynolds-number turbulent jet at Mach 0.9," *J. Fluid Mechanics*, vol. 438, pp. 277-305.

Fisher, M. J., Harper-Bourne, M. and Glegg, S.A.L., (1977) "Jet Engine Source Location: The Polar Correlation Technique," *J. Sound and Vibration*, Vol. 51, No. 1, pp. 23-54.

Hileman, J. and Samimy, M., "Turbulence Structures and the Acoustic Far-Field of a Mach 1.3 Jet," *AIAA J.*, Vol. 39, No. 9, 2001, pp. 1716-1727.

Hileman, J., Thurow, B. and Samimy, M., (2002) "Exploring Noise Sources Using Simultaneous Acoustic Measurements and Real-Time Flow Visualizations in Jets," *AIAA J.*, Vol. 40, No. 12, pp. 2382-2392.

Hileman, J. and Samimy, M., (2003) "Effects of Vortex Generating Tabs on Noise Sources in an Ideally Expanded Mach 1.3 Jet," *International J. Aeroacoustics*, Vol. 2, No. 1, pp. 35-63.

Hileman, J., Thurow, B. and Samimy, M., (2004) "Development and Evaluation of a 3-D Microphone Array to Locate Individual Acoustic Sources in A High-speed Jet," accepted to *J. Sound and Vibration*, accepted August 2003, pending publication in 2004.

Hileman, J., (2004) *Large-Scale Structures and Noise Generation in High-Speed Jets*, Ph.D. Dissertation, The Ohio State University Department of Mechanical Engineering.

Hussain, A.K.M.F., (1986) "Coherent Structures and Turbulence," *J. Fluid Mechanics*, Vol. 173, pp. 303-356.

Lee, H.K. and Ribner, H.S., (1972) "Direct correlation of noise and flow of a jet," *J. Acoustical Society America*, Vol. 52, pp. 1280-1290.

Lighthill, M.J., (1952) "On Sound Generated Aerodynamically. Part I: General Theory." *Proc. Royal Soc. London*, Ser. A., Vol. 211, pp. 564-587.

Lighthill, M.J., (1954) "On Sound Generated Aerodynamically. Part II: Turbulence as a Source of Sound" *Proc. Royal Soc. London*, Ser. A., Vol. 222, pp. 1-32.

Lilley, G.M., (1991) "Jet Noise Classical Theory and Experiments," *Aeroacoustics of Flight Vehicles: Theory and Practice*. Vol. 1, ed. H.H. Hubbard, pp. 211-290. NASA RP-1258.

Lumley, J., (1967) "The Structure of Inhomogeneous Turbulent Flows," *Atmospheric Turbulence and Wave Propagation*, edited by A.M. Yaglow and V.I. Tatarski, Moscow: Nauka, pp. 166-176.

Morrison, G. and McLaughlin, D., (1979) "Noise Generation by Instabilities in Low Reynolds Number Supersonic Jets," *J. Sound and Vibration*, Vol. 65, pp. 177-191.

Neise, W. and Enghardt, L., (2003) "Technology approach to aero engine noise reduction," *Aerospace Science and Technology*, Vol. 7, pp. 352-363.

Panda, J. and Seasholtz, R.G., (2002) "Experimental investigation of density fluctuations in high-speed jets and correlation with generated noise," *J. Fluid Mechanics*, Vol. 450, pp. 97-130.

Sarohia, V. and Massier, P.F., (1977) "Experimental Results of Large-scale Structures in Jet Flows and Their Relation to Jet Noise Production," AIAA Paper 77-1350.

Schaffar, M., (1979) "Direct Measurements of the Correlation Between Axial in-jet Velocity Fluctuations and Far-field Noise near the Axis of a Cold Jet," *J. Sound and Vibration*, Vol. 64, No. 1, pp. 73-83.

Siddon, J.E., (1973) "On noise mechanisms. Noise source diagnostics using causality correlation," AGARD CP 131.

Simonich, J., Narayanan, S., Barber, T.J. and Nishimura, M., "Aeroacoustic Characterization, Noise Reduction, and Dimensional Scaling Effects of High Subsonic Jets", *AIAA J.*, Vol. 39, No. 11, 2001, pp. 2062-2069.

Sirovich, L., (1987) "Turbulence and the Dynamics of Coherent Structures, Part I: Coherent Structures," *Quarterly Applied Math*, Vol. XLV, No. 3, pp. 561-571.

Sirovich, L. and Everson, R., (1992) "Management and Analysis of Large Scientific Datasets," *International J. Supercomputer Applications*, Vol. 6, No. 1, pp. 50-68.

Sirovich, L. and Kirby, M., (1987) "Low-dimensional procedure for the characterization of human faces," *J. Optical Society of America A*, Vol. 4, No. 3, pp. 519-523.

Stromberg, J., McLaughlin, D. and Troutt, T., (1980) "Flow field and acoustic properties of a Mach number 0.9 jet at a low Reynolds number," *J. Sound and Vibration*, Vol. 72, No. 2, pp. 159-176.

Tam, C.K.W., (1991) "Jet Noise Generated by Large-Scale Coherent Motion," *Aeroacoustics of Flight Vehicles: Theory and Practice*. Vol. 1, ed. H.H. Hubbard. pp. 311-390, NASA RP-1258.

Thurow, B., Hileman, J., Samimy, M. and Lempert, W., (2002) "A technique for real-time visualization of flow structure in high-speed flows," *Phys. Fluids*, Vol. 14, No. 10, pp. 3449-3452.

Thurow, B., Samimy, M. and Lempert, W., (2003) "Compressibility Effects on Turbulence Structures of Axisymmetric Mixing layers," *Phys. Fluids*, Vol. 15, No. 6, pp. 1755-1765.

Ukeiley, L. and Seiner, J., (1998) "Examination of Large-scales Structures in a Transonic Jet Mixing layer," ASME FEDSM 98-5234.

Venkatesh, S., Polak, D. and Narayanan, S., (2003) "Beamforming Algorithm for Distributed Source Localization and its Application to Jet Noise," *AIAA J.*, Vol. 41, No. 7, pp. 1238-1246.

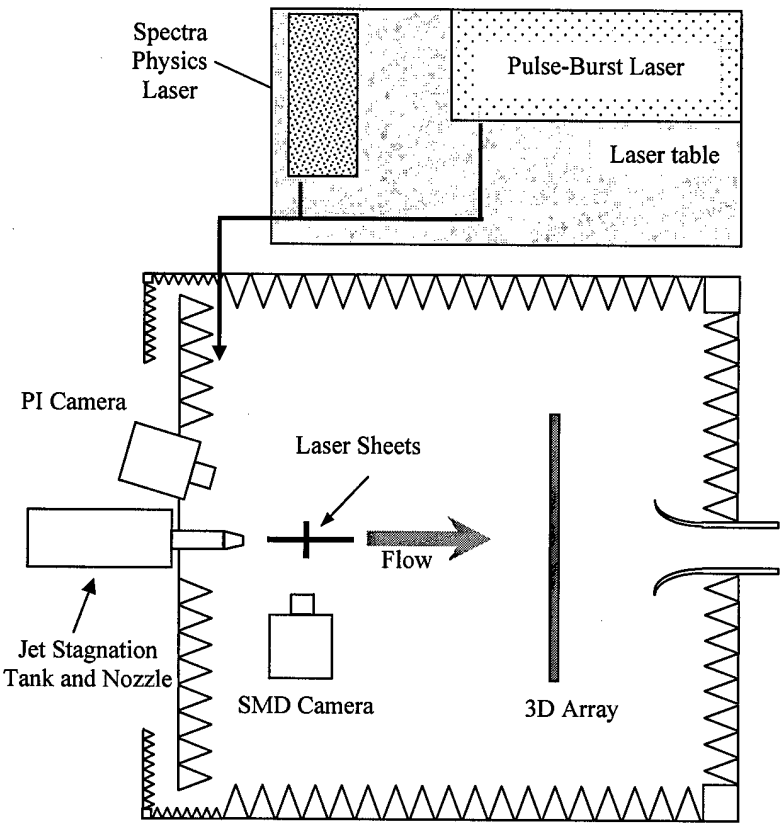

Figure 1: Schematic of the facility and equipment used in the simultaneous flow / acoustic experiments. Figure is not to scale.

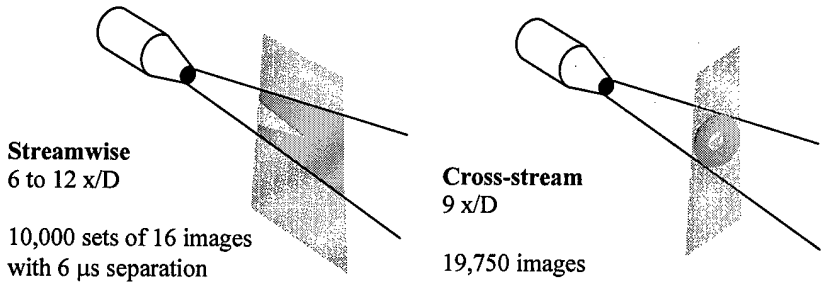

Figure 2: Schematics of the two laser sheet orientations used in this study as well as images of the illuminated flow.

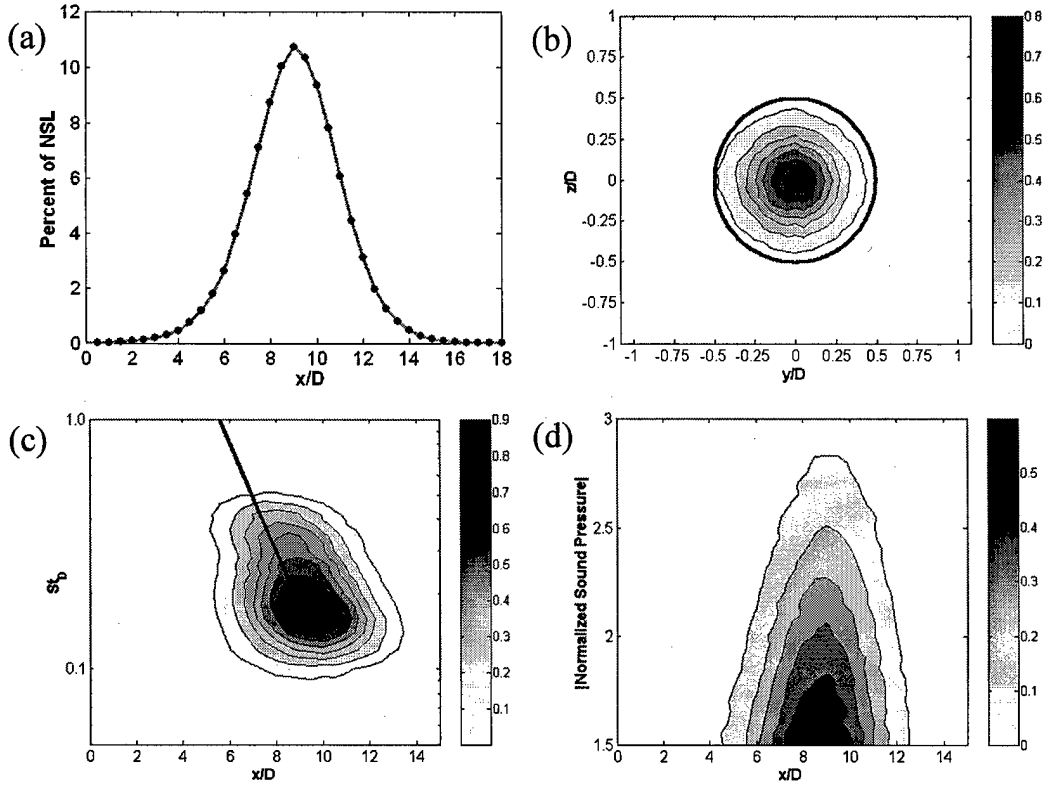

Figure 3: Noise source location data from the Mach 1.3 jet. The streamwise probability distribution is shown in (a) while (b) gives the two-dimensional, cross-stream distribution. Strouhal number (c) and sound pressure magnitude (d) are shown as functions of downstream distance. The black line of (c) is a noise source location fit to the data of Venkatesh et al. [2003].

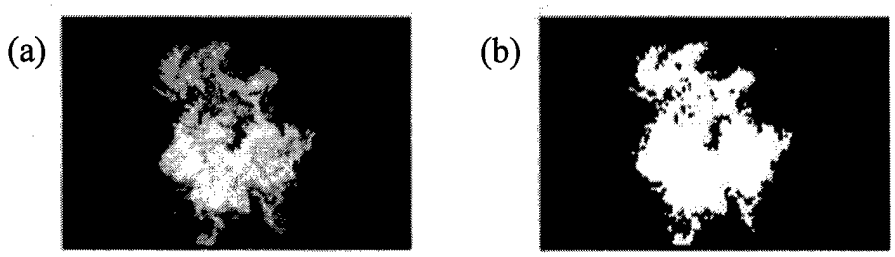

Figure 4: Cross-stream instantaneous image (a) and the image after conversion to binary (b). Binary images were used for statistical and POD processing.

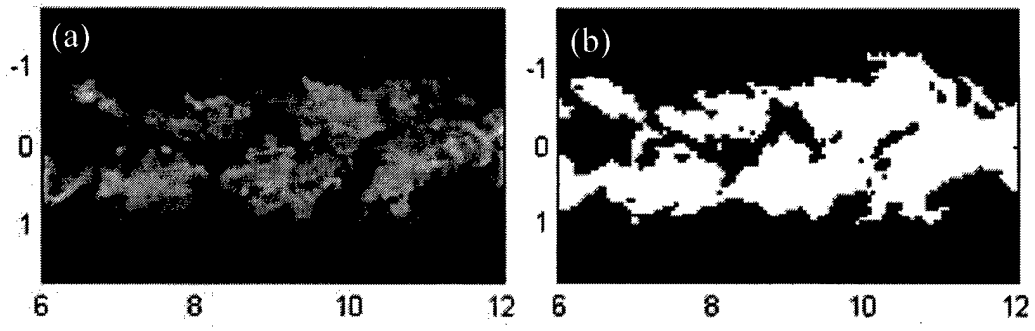

Figure 5: Streamwise images that show the intensity of the raw image (a) and the same image after conversion to binary (b). Binary images were used for statistical and POD processing.

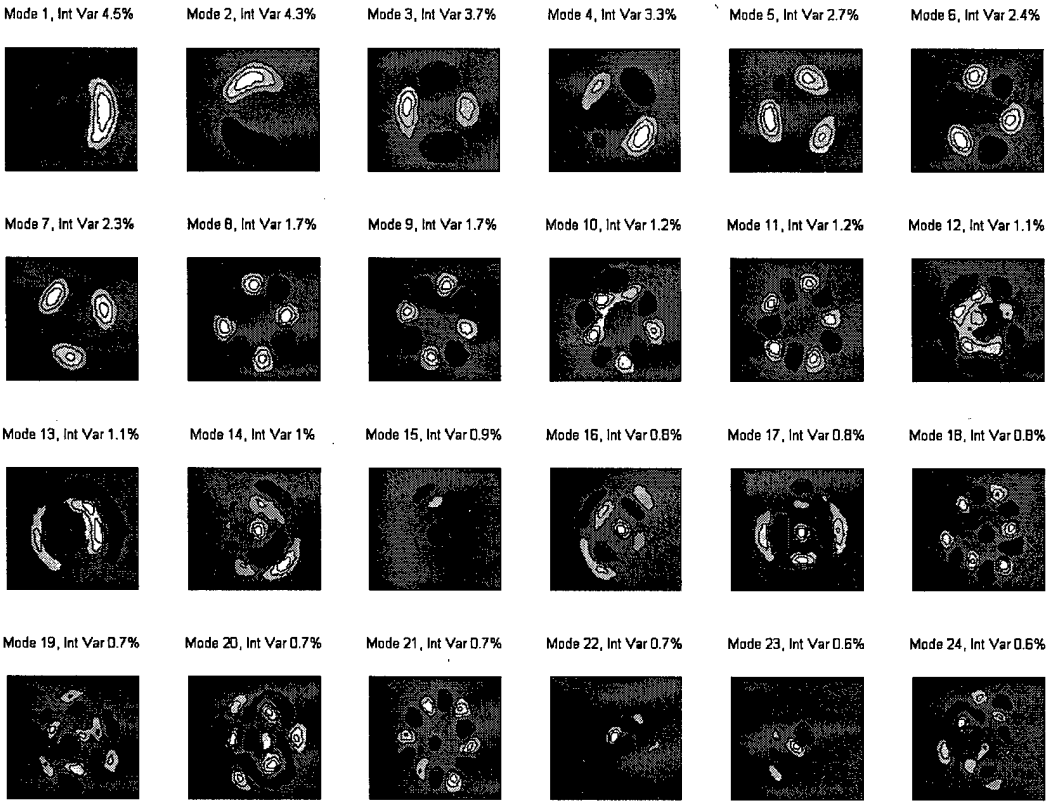

Figure 6: POD modes created from 2000 images of the cross-stream plane at 9 x/D using the intensity fluctuations from the mean. White and black show opposite sign fluctuations.

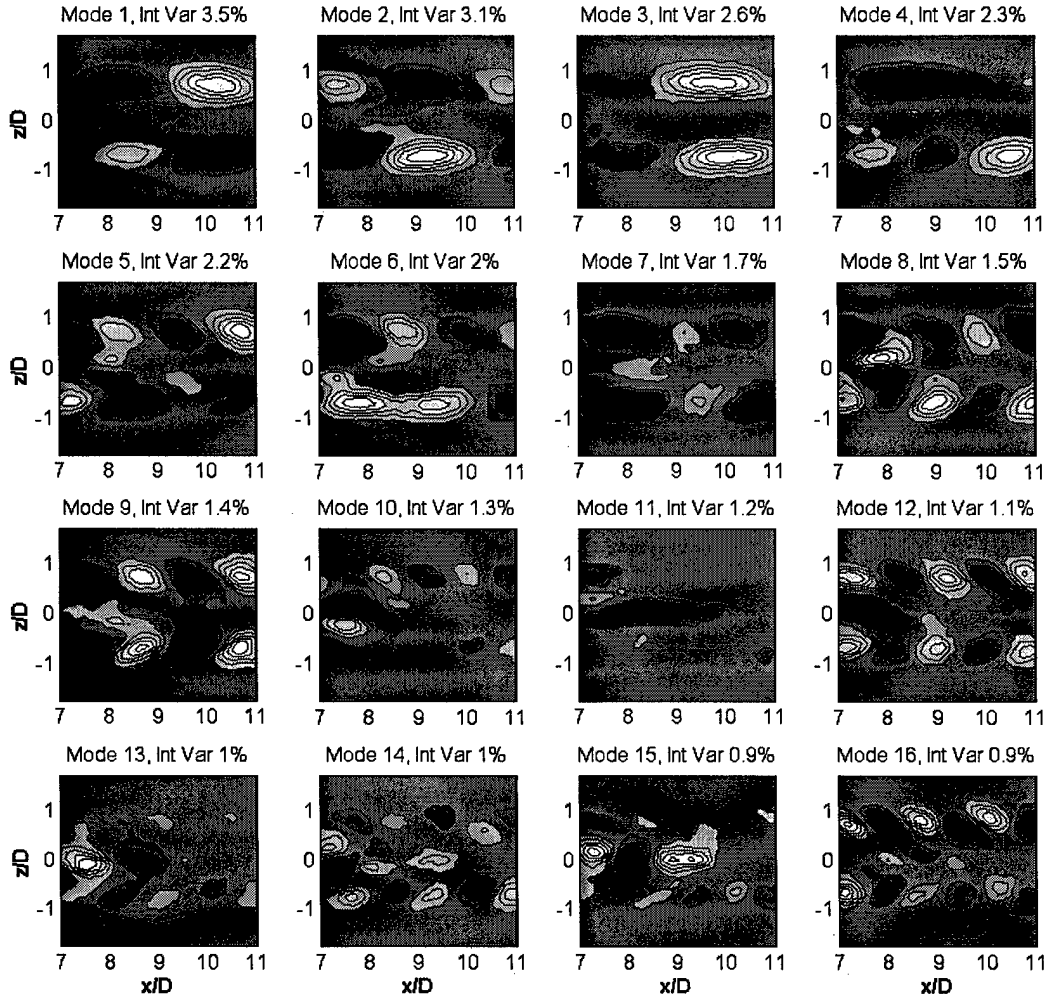

Figure 7: POD modes created from 2000 images of the streamwise plane between 7 and 11 x/D using the intensity fluctuations from the mean intensity.

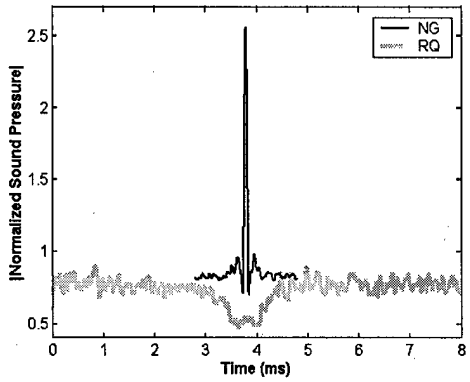

Figure 8: Absolute value of normalized sound pressure from ensemble averaged noise generation (NG) and from a lack of noise generation (RQ) signals reaching the microphone array.

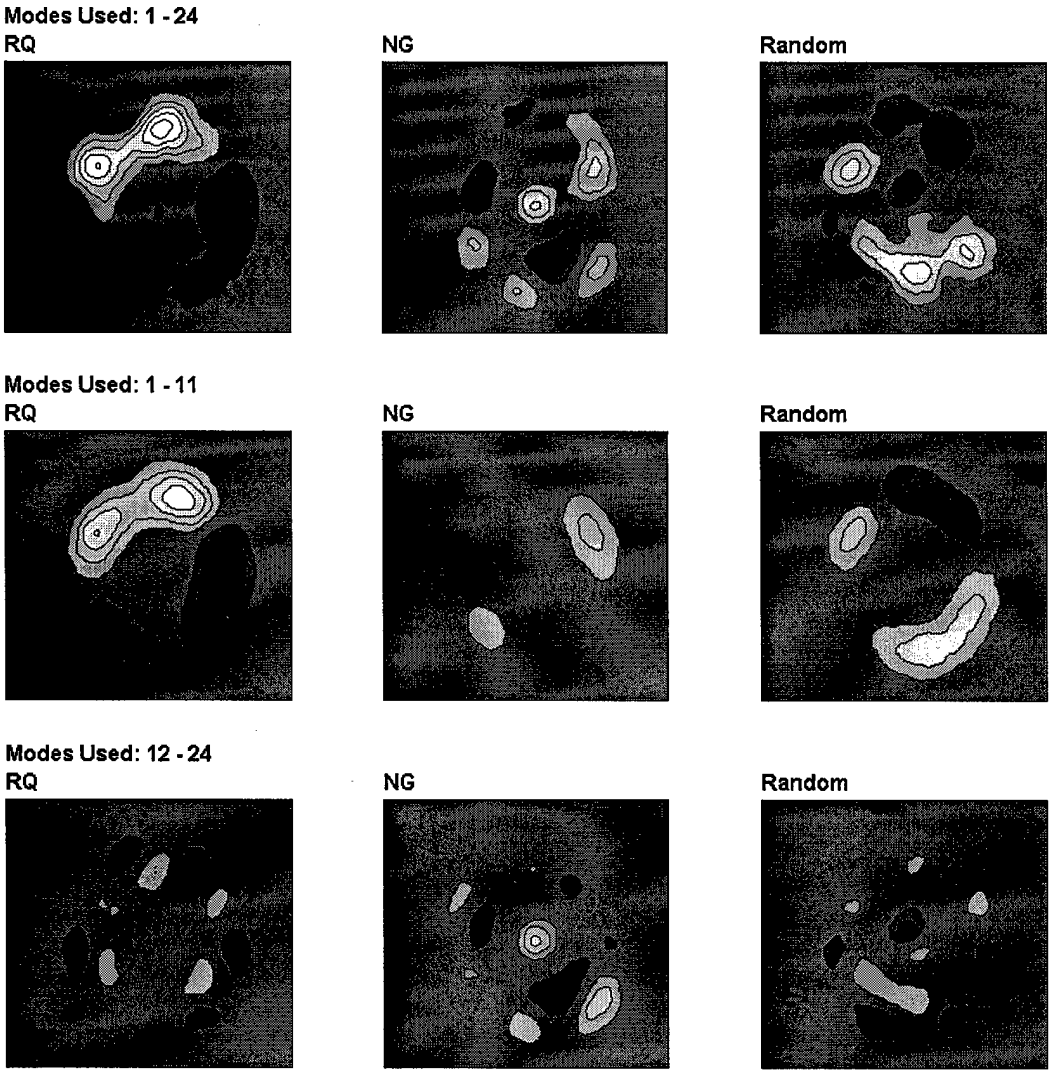

Figure 9: Average of 200 reconstructed images from the RQ, NG, and random sets of cross-stream flow images. Three sets of POD modes were used in the reconstruction: 1-24 (all), modes 1-11 and modes 12-24.

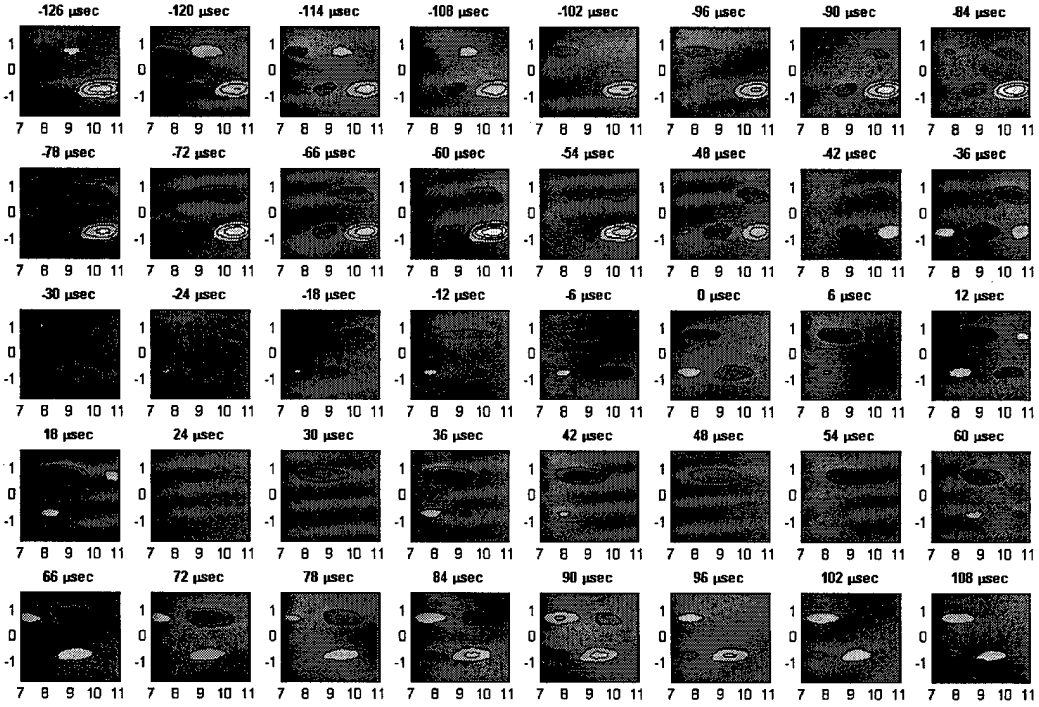

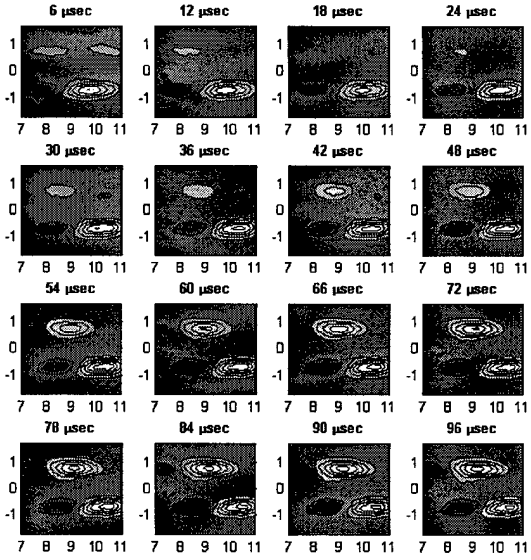

Figure 10: Reconstructed images for streamwise NG (above) and RQ (right) states using modes 1 to 4.

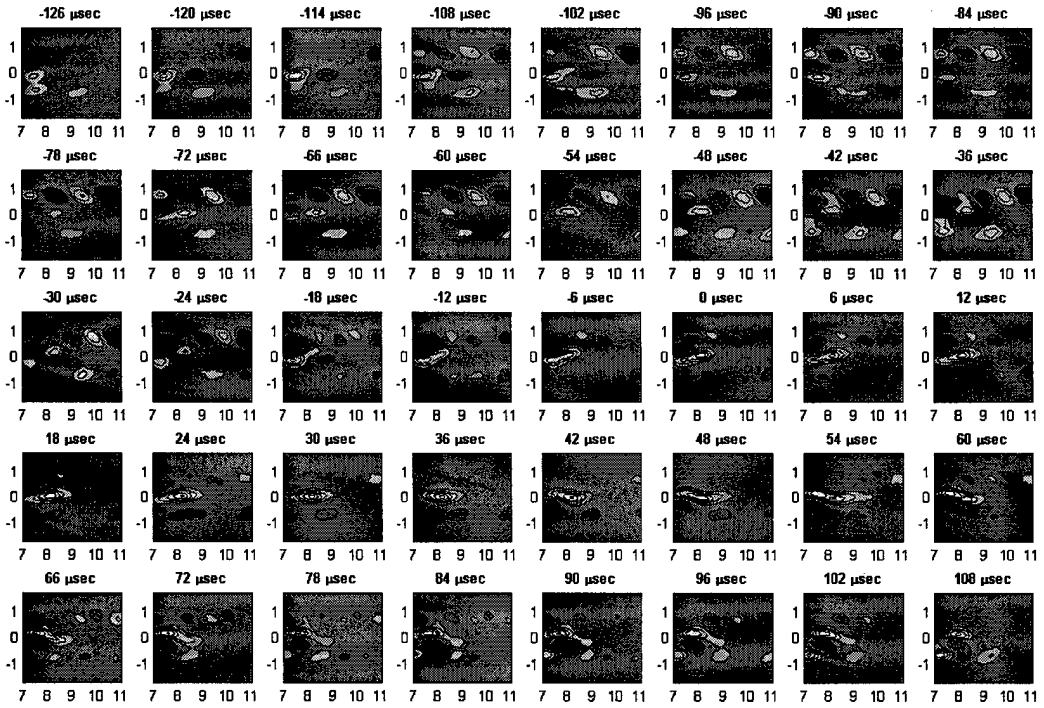

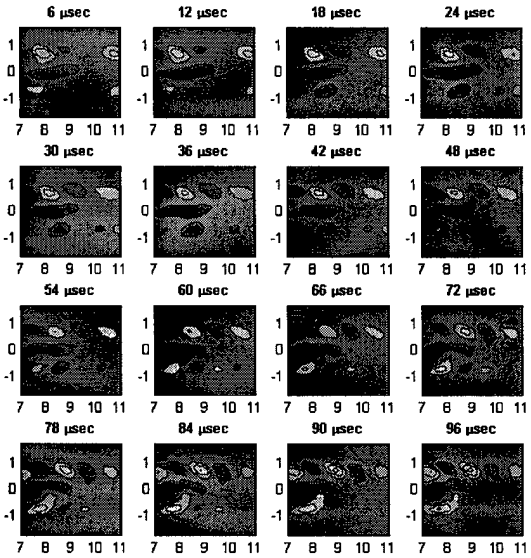

Figure 11: Reconstructed images for streamwise NG (above) and RQ (right) states using modes 5 to 16.